IEEE Open Journal of
Power Electronics

Received 16 December 2022; revised 25 January 2023; accepted 12 February 2023. Date of publication 20 February 2023;
date of current version 14 March 2023. The review of this article was arranged by Associate Editor Lina He.

Digital Object Identifier 10.1109/OJPEL.2023.3246728

Voltage-Based Current Limitation Strategy to Preserve Grid-Forming Properties Under Severe Grid Disturbances

ANANT NARULA [1] (Student Member, IEEE), PAUL IMGART [1] (Student Member, IEEE), MASSIMO BONGIORNO [1] (Senior Member, IEEE), MEBTU BEZA [1] (Member, IEEE), JAN R. SVENSSON [2] (Senior Member, IEEE), AND JEAN-PHILIPPE HASLER [3]

[1]Department of Electrical Engineering, Chalmers University of Technology, 412 96 Göteborg, Sweden
[2]Hitachi Energy Research, Hitachi Energy, 722 26 Västerås, Sweden
[3]Hitachi Energy, 721 64 Västerås, Sweden

CORRESPONDING AUTHOR: ANANT NARULA (e-mail: anant.narula@chalmers.se)

ABSTRACT Grid-forming (GFM) converters are a promising solution to enable large scale integration of renewable energy sources into the power system. However, due to the intrinsic voltage-source behaviour of GFM converters, current limitation during large grid disturbances is challenging. This article presents a novel limitation strategy that preserves the GFM properties of the converter and at the same time effectively limits the converter current to the desired value. Through the limitation of the converter's internal voltage, stable operation even during faults and in case of large frequency disturbances in the grid is achieved. Experimental results show the effectiveness of the proposed current limitation strategy in case of various grid disturbances.

INDEX TERMS Current limitation, grid-forming converter, grid-connected converter, transient stability, unbalanced faults, virtual inertia.

I. INTRODUCTION

In the 2015 Paris Agreement on climate change, 189 signature states have agreed to limit global temperature rise to below 2 °C by the end of the century, and to aim for 1.5 °C [1]. A crucial part of these efforts is the decarbonization of the electrical power systems worldwide by using renewable power sources, which are commonly interfaced to the grid by power-electronic converters. Trends such as higher utilization and flexibility demands on power system assets accompanied by stronger interconnections between different systems, as well as the proliferation of drive systems and consumer electronics, further increase the share of power electronics in the grid [2]. This development has raised concerns about the stability and feasibility of converter dominated grids [3]. Grid-forming (GFM) converters emulate the voltage-source behaviour of synchronous machines [2], [3], [4], [5], [6], [7], and are widely discussed as a solution to the challenges associated with increased penetration of converter-based resources [2], [3], [8]. A common element of most GFM converter designs is that the active power transfer is used for synchronization to the grid, replacing the phase locked-loop (PLL) typically used in the more conventional grid-following control [9].

As power-electronic converters have limited overcurrent capability, the ability to limit the current not only during normal operation but also during grid disturbances is a necessity for all converter control schemes. In contrast to grid-following control, GFM-based converters are controlled to emulate a voltage source behind an impedance; as a consequence, the current exchanged between the converter and the grid is indirectly controlled and thereby its limitation is challenging [10], [11]. Current limitation is typically reached during large grid disturbances, such as faults or large frequency excursions, during which the grid is most vulnerable and in need of support. For this reason, the converter should retain as much of the GFM behavior as possible even during current limitation. This implies that, if at all necessary, the converter dynamic properties should be changed for the shortest time possible, typically up to a few cycles at fundamental frequency; then the converter should return into linear control mode [12], [13].

Various current-limitation strategies have been investigated and reported in the literature in the recent years; these can be summarized into four main categories [10]:

- *Immediate current limitation:* This method is commonly applied in cascaded voltage and current vector controllers [14], [15], [16] and in virtual admittance control [17], [18], [19], since both control schemes contain an explicit current reference and a current controller (CC). The approach requires a CC that is active at least during current limitation, so that the controller's current reference can be limited. As described more in detail in the following section, stability problems can occur under severe grid disturbances [20] if this method is used.
  A variation of this scheme is applied in power synchronization control [21], [22], where the CC is only activated when the current limiter saturates. Thus, the synchronization task switches from the active-power loop (APL) to a PLL, and the converter behaves as a current source instead of a voltage source during limitation.
- *Indirect current limitation by virtual impedance:* GFM converters behave as a voltage source behind an impedance, and a (virtual) increase of the impedance reduces the current exchanged with the grid. The virtual impedance based limitation approach [23], [24], [25], [26] can be realized with or without a current control loop [10]. The method's main challenge is that the selection of virtual impedance parameters requires system knowledge and assumptions regarding the worst case. System conditions differing from those assumptions can result in overcurrent or low utilization of the converter fault current contribution capability [10]. Moreover, an adaptive virtual impedance can result in system instability [27].
- *Indirect current limitation by voltage limitation:* A different approach to limit the current in a GFM converter is to vary the converter's virtual-back electromotive force (EMF) voltage instead of the impedance, which can be implemented in different ways. Some require knowledge of the grid voltage angle [28], [29], which in practice can result in mode-switching into PLL-based synchronization. In [30], only the magnitude of the voltage reference is limited. A power reference limiter is used to prevent overcurrent due to excessive load angles, but the issue of instability due to frequency disturbances remains unsolved.
- *Indirect current limitation by power limiter:* Here, the input to the active- and reactive-power control loops is limited to prevent overcurrent [18], [31], [32]. These methods rely on fault detection, which is challenging for disturbances where the voltage magnitude remains unaffected. Furthermore, for controllers with slow outer control loops, overcurrent can not be prevented reliably during transients [10].

In addition to the challenges described above, it is important to highlight that the majority of the studies available in the literature focus on current limitation and transient stability for GFM converters in case of voltage dips [18], [33], [34], [35], [36], [37], [38], [39], [40]; on the other hand, large frequency disturbances can also be a significant source of instability, especially when high-inertia support is demanded from the converter [41]. The referred methods for current limitation do not address the impact of limitation on robustness against frequency disturbances.

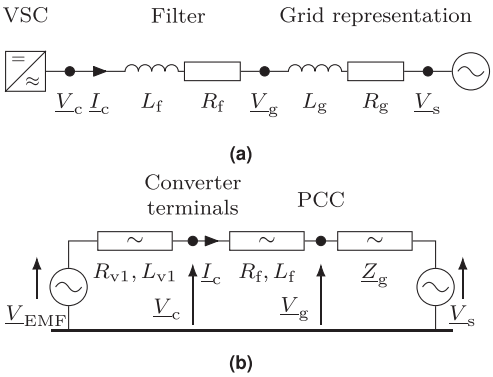

FIGURE 1. (a): Single-line diagram of the investigated system. (b): Equivalent circuit representation of a GFM converter control approach with virtual-back EMF and virtual impedance.

This article presents a novel current limitation strategy for GFM converters that ensures accurate current limitation during symmetric and asymmetric faults as well as during frequency disturbances and phase jumps; through adequate limitation of the reference active power and magnitude of the virtual-back EMF reference, the proposed strategy does not require any system knowledge and retains the converter's GFM properties even during current limitation.

The article is structured as follows: Section II is a theoretical study of the GFM converter transient stability problem. In Sections III and IV, the basic converter control and the proposed limitation strategy are presented, respectively. Section V contains the experimental verification of the proposed strategy, and the conclusions are put forward in Section VI.

II. GFM CONVERTER ANGLE STABILITY PROBLEM

The GFM converter angle stability problem is analyzed by using the system in Fig. 1. It consists of a GFM converter with a virtual-back EMF $\underline{V}_{EMF}$ and a virtual impedance R_v, L_v. The virtual impedance includes the converter filter impedance and the virtual part R_{v1}, L_{v1}. The *R-L* filter connects the converter terminals at the point of common coupling (PCC) to the grid, which is represented by the Thévenin equivalent $\underline{V}_s$ and $\underline{Z}_g$. Neglecting the system losses, the steady state per-unit converter current in the synchronous reference frame aligned with the converter's virtual-back EMF voltage is

$$\underline{I}_c = \frac{\underline{V}_{EMF} - \underline{V}_s}{jX} = \frac{V_s \sin\delta + j(V_s\cos\delta - V_{EMF})}{X}, \quad (1)$$

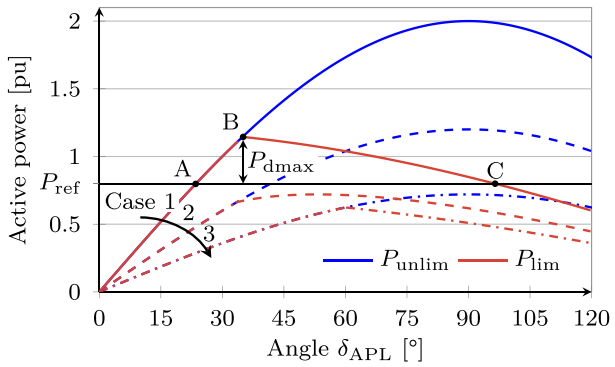

FIGURE 2. ***P*-δ_{APL} curve illustrating the converter angle stability problem for a current limit of 1.2 pu. A: pre-disturbance operating point; B: current limit reached; C: transient stability limit; P_{dmax}: maximum decelerating power; all outlined for case 1: $V_{EMF} = V_s = 1$ pu. Case 2: $V_{EMF} = 1$ pu & $V_s = 0.6$pu; case 3: $V_{EMF} = V_s = 0.6$ pu.**

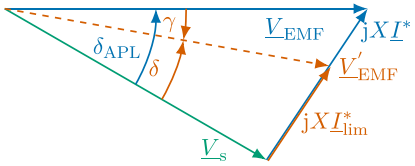

FIGURE 3. **Phasor diagram illustrating the effect of current limitation on the virtual-back EMF. Unlimited in blue, limited in red.**

where $\delta = \angle\underline{V}_{EMF} - \angle\underline{V}_s$, and X is the total reactance between the two sources. The active-power transfer from the converter to the grid is defined as

$$P = \Re\mathfrak{e}\{\underline{V}_{EMF}\,\mathrm{conj}\{\underline{I}_c\}\} = \frac{V_s V_{EMF}}{X}\sin\delta, \tag{2}$$

and shown in blue in Fig. 2 for an example system.

The current exchanged with the grid needs to be limited to prevent damage to the converter hardware due to overcurrent. Following the immediate current limitation approach introduced in the previous section, a CC is used and its reference is limited with a current-magnitude limiter [10] (also addressed as circular-current limiter [18]). Applying this to limit the current reference $\underline{I}^*$ to the maximum allowed converter current I_{max} yields

$$\underline{I}^*_{lim} = \underline{I}^*\frac{I_{max}}{I^*} \qquad \forall I^* > I_{max} \tag{3}$$

as the limited converter current reference. This current limitation is equivalent to a variation of the phasor $\underline{V}_{EMF}$, defined as $\underline{V}'_{EMF}$ in the phasor diagram in Fig. 3. The figure shows that the current limitation results in a reduction of the load angle δ when compared with the angle of the unlimited output of the APL, denoted as δ_{APL}. Even though the load angle is manipulated by the current limitation, the APL's output angle δ_{APL} still has an impact on the exchanged active power by determining the angle of the current references $\underline{I}^*$ and consequently $\underline{I}^*_{lim}$. Using (1)–(3), the relation between the current-limited active power P_{lim} and the APL output angle δ_{APL} can be determined by

$$\begin{aligned} P_{lim} &= \Re\mathfrak{e}\{\underline{V}_s\,\mathrm{conj}\{\underline{I}^*_{lim}\}\} \\ &= \frac{V_s V_{EMF} I_{max}\sin\delta_{APL}}{\sqrt{V_s^2 + V_{EMF}^2 - 2V_s V_{EMF}\cos\delta_{APL}}}, \qquad I^* > I_{max} \end{aligned} \tag{4}$$

Fig. 2 illustrates the current-limited *P*-δ_{APL} relationship following from (4) in red. The current reaches its limit at operating point B, and in contrary to the unlimited case presented in blue increasing δ_{APL} further results in a decreasing power transfer.

Based on this analysis, the two main sources for GFM converter angle instability [41] can be studied: firstly, an active power reference that during a fault or in post-fault steady-state is too large for the grid conditions (i.e. grid voltage magnitude and grid strength), and secondly the inability of the APL to follow the grid voltage angle in case of a frequency disturbance or phase-angle jump. The former is studied widely in the literature [18], [33], [35], [36], [37], [38], [40], while the latter is rarely regarded in existing publications [41]. Both instability mechanisms are summarized in this section.

A. VOLTAGE-DIP INDUCED CONVERTER ANGLE INSTABILITY

The first of the two angle instability mechanisms is caused by a voltage dip at the PCC. Equations (2) and (4) demonstrate that the active-power transfer between converter and grid is proportional to the product of V_s and V_{EMF}. Consequently, a voltage dip will result in a reduced active power transfer capability, no matter how the converter back EMF magnitude is controlled in response to the voltage dip (compare case 2 and 3 in Fig. 2). As described in [27], instability can under this conditions occur due to violated equal-area criterion, which mainly affects GFM converters providing inertial support, or due to lack of a stable post-fault operating point. This type of instability has been studied widely in literature and several solutions have been proposed [38]. The most popular solutions are scaling of the power references proportional to the voltage magnitude [18], control-mode switching (e.g. deactivation of inertia [42]), inclusion of additional control terms [43] and moving to a grid-following control mode [22]. Of these approaches, voltage-proportional power reference scaling has the advantage of retaining as much of the GFM capabilities as possible, while at the same time aiding in current-limitation. In contrast to approaches modifying the control structure, it does not require any fault detection [38].

B. FREQUENCY-DISTURBANCE INDUCED CONVERTER ANGLE INSTABILITY

The second angle instability mechanism is caused by severe frequency disturbances or phase angle jumps in the grid, resulting in the inability of the APL to follow the grid voltage angle and moving the operating point to the unstable part in Fig. 2. This phenomenon is discussed more in-depth in [41]. As the APL in a GFM converter does not only provide power reference tracking but also synchronization, a power

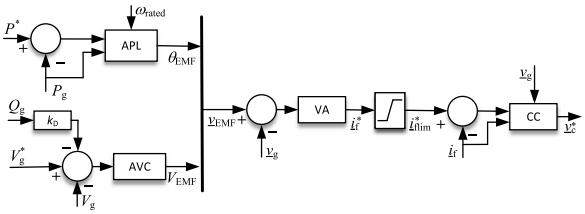

FIGURE 4. Block diagram of investigated GFM control structure.

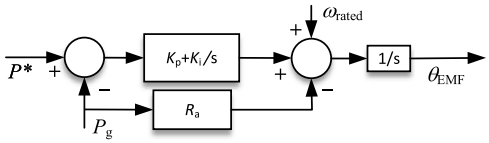

FIGURE 5. Block diagram of implemented active power loop (APL).

control error is required to follow a change in the grid frequency by letting the APL adapt its internal frequency. For instance, a decline in grid frequency causes the load angle δ to increase until the additional decelerating power $P_\mathrm{d} = -2H\frac{\mathrm{d}\omega}{\mathrm{d}t}$ is reached. During current limitation the decelerating power might not be large enough to keep the converter's internal frequency synchronized with the grid frequency, which would lead to the load angle continuing to increase. If the unstable equilibrium point C is passed synchronism is lost, equivalent to synchronous machine first swing instability.

Limitation of the outer loop references as introduced in the previous instability mechanism cannot prevent loss of synchronism in this case. This is because the active power exceeding the current-limited maximum is not caused by a change in reference, but by the inability of the slow APL to reject the grid disturbance. This slowness is desired to provide inertia to the grid, but causes instability when the converter current limits are reached. Not only the GFM control structure used for illustration in this section, but all GFM converters with non-zero inertia that rely on the APL for synchronization and provision of inertia are vulnerable to this type of instability. As the APL angle output is manipulated to guarantee current limitation, the synchronization signal is lost. The risk for this type of instability is increased by large inertia, high rate of change of frequency (RoCoF) and operating points close to the maximum power transfer, due to more decelerating power being needed or less current reserve being available for it, respectively.

While these instability mechanisms are studied here for a GFM converter with circular-current limitation, the same principles apply for GFM converters relying on a virtual impedance for current limitation. This can be understood from (2), showing that an increase in the reactance between the virtual-back EMF and the grid voltage will reduce the active-power transfer for any given load angle, which results in similar dynamics for both instability types.

III. BASIC GFM CONVERTER CONTROL

The GFM control adopted in this work is based on the virtual admittance-based approach from [19], with the improvements to the APL described in [41]. The controller implementation is illustrated in Fig. 4 and its main blocks are described in the following.

A. ACTIVE POWER LOOP (APL)

For the investigated GFM control, the APL provides both active-power reference tracking and grid synchronization. The implemented APL is depicted in Fig. 5 and consists of a PI regulator for accurate reference tracking and an active-damping term R_a to improve the controller's dynamic performance. Neglecting the system's losses, the maximum transmittable active power is given by:

$$P_\mathrm{max} = \frac{V_\mathrm{EMF}V_\mathrm{g}}{X_\mathrm{v}},$$

where X_v is sum of the converter's virtual reactance X_v1 and filter reactance X_f. Using the controller active damping R_a and the proportional and integral gains K_p and K_i, the closed-loop transfer function for the APL can be written as

$$G_\mathrm{PC}(s) = \frac{K_\mathrm{p}s + K_\mathrm{i}}{P_\mathrm{max}^{-1}s^2 + (K_\mathrm{p} + R_\mathrm{a})s + K_\mathrm{i}}, \tag{5}$$

assuming that the CC is sufficiently fast to be treated as ideal. The APL control parameters are tuned using loop-shaping approach as described in [41] to yield

$$G_\mathrm{PC}(s) = \frac{\alpha_\mathrm{PC}}{s + \alpha_\mathrm{PC}} \tag{6}$$

with

$$K_\mathrm{p} = \frac{\alpha_\mathrm{PC}}{P_\mathrm{max}}, \quad K_\mathrm{i} = \frac{\alpha_\mathrm{PC}^2}{P_\mathrm{max}}, \quad \text{and} \quad R_\mathrm{a} = K_\mathrm{p},$$

where α_PC denotes the desired APL closed-loop bandwidth.

B. AC VOLTAGE CONTROLLER (AVC)

The magnitude of the virtual-back EMF is determined by the AC voltage controller (AVC), which controls the voltage at the PCC. To allow operation in strong grids and alongside other converters, an integral controller with a reactive droop is used. Denoting with V_N the nominal grid voltage and with k_D the droop constant, the control law for the AVC is defined by [19]:

$$V_\mathrm{EMF} = V_\mathrm{N} + \frac{K_\mathrm{iv}}{s}(V_\mathrm{g}^* - V_\mathrm{g} - k_\mathrm{D}Q_\mathrm{g}), \tag{7}$$

where, for a desired closed-loop bandwidth α_VC, $K_\mathrm{iv} = \alpha_\mathrm{VC}\frac{X_\mathrm{v}+X_\mathrm{g}}{X_\mathrm{g}}$. The value of the grid reactance, X_g, used for calculating the integral gain of the AVC is typically set for the strongest grid strength provided by the system operator, to ensure an acceptable performance even with varying grid strengths.

C. VIRTUAL ADMITTANCE (VA)

The virtual-back EMF voltage vector determined by the outer loops is translated into a current reference input for the CC by a virtual admittance (VA)[1]. The VA generates the reference currents by providing filtering and damping action (through L_v and R_v, respectively) on the difference between the virtual-back EMF and the grid voltage. It also reduces the impact of variations in grid strength on the converter dynamic performance by reducing the share of the grid impedance in the total impedance [44]. As proposed in [17], the virtual reactance is chosen in the range of a typical synchronous machine transient reactance. Due to this relatively large virtual reactance, changes in the virtual-back EMF result in a DC current component. The virtual resistance is chosen to provide a small time constant for the decay of this current offset. The current reference output of the VA block is:

$$\underline{i}_f^* = \frac{\underline{v}_{EMF} - \underline{v}_g}{sL_v + j\omega_N L_v + R_v}. \tag{8}$$

D. CURRENT CONTROLLER (CC)

The current references generated by the VA are limited to the maximum converter current as in (3) and sent to the CC to calculate the reference voltages for the converter's modulation stage. The implemented CC has a classical structure and is based on a PI regulator with cross-coupling cancellation and voltage feedforward that is low-pass filtered with a closed-loop bandwidth of α_{FF} as:

$$\underline{v}_c^* = \frac{\alpha_{FF}}{s+\alpha_{FF}}\underline{v}_g + j\omega_N L_f \underline{i}_f + (K_{pc} + \frac{K_{ic}}{s})\left(\underline{i}_f^* - \underline{i}_f\right). \tag{9}$$

The controller gains are tuned to the selected controller bandwidth α_{CC} as [45]

$$K_{pc} = \alpha_{CC} L_f, \quad K_{ic} = \alpha_{CC} R_f. \tag{10}$$

IV. PROPOSED METHODOLOGY TO LIMIT CONVERTER CURRENT

From Section II, it is understood that limitation of the current reference for the CC (henceforth referred to as hard-current limiter) might in GFM converters result in a loss of synchronization with the AC grid. Furthermore, the use of the hard-current limiter introduces non-linearities in the control system and modifies the dynamic properties of the converter (by hiding the impact of the voltage controller and the virtual admittance) while activated, which is not desirable as discussed earlier [12], [13]. This section presents a novel strategy that allows to keep the converter current within its permissible value without relying on the hard-current limiter and alteration of the GFM properties.

In a grid-following converter, the use of a hard-current limiter is effective because such converters are modeled as a current source. Following the same philosophy for GFM converters, which are modeled as a voltage source instead, current limitation can be achieved by dynamically limiting the generated virtual-back EMF, $\underline{v}_{EMF}$, so that the resulting current reference is within the limits. This is realized through the GFM control structure depicted in Fig. 6. It is of importance to consider that, unlike the magnitude, limiting the phase of the voltage vector $\underline{v}_{EMF}$ is challenging. This is because in the absence of a PLL in GFM converters, there is no direct information about the load angle; and hence, the active-power flow from the converter dictates the phase of the emulated voltage source. Therefore, one obvious solution is to include a PLL in the design of the APL to calculate the converter's load angle. However, this can have a negative impact on the stability of the converter in weak grids, and restrict the converter's GFM properties [46]. Another alternative to limit the resulting phase of the converter at all times without the aforementioned restrictions is to limit the active-power reference. However, as discussed in Section II-B, this solution is not effective in GFM converter systems emulating inertia, owing to their slow APL. To overcome this issue, the cascaded active-power controller described in the following section is used. The calculation of the limits for the active power and voltage magnitude references is described in the subsequent sections.

A. CASCADED ACTIVE-POWER CONTROLLER

The cascaded active-power controller consists of an inertia-emulation loop (IEL) in cascade with a fast APL, as first reported in [41]. The IEL is illustrated in Fig. 7 and is based on the structure of a PLL. It is used to calculate the inertial power, P_H, to be injected (or absorbed) by the converter in case of frequency disturbances. As from the figure and denoting with θ_g the angle of the PCC voltage $\underline{v}_g$, the inertial power output from the IEL is given by

$$P_H = -\frac{V_g V_c}{X_f}\sin(\theta_g - \theta_{IEL}), \tag{11}$$

where $\theta_g = \theta_{IEL}$ in steady state. In the case of a frequency variation, the IEL angle will track the grid angle with a speed of response determined by the desired amount of emulated inertia H. For this, the IEL's proportional ($K_{p,IEL}$) and integral ($K_{i,IEL}$) gains are selected as [41]

$$K_{p,IEL} = \zeta\sqrt{\frac{2\omega_N X_f}{HV_{cr}V_{gr}}},\ K_{i,IEL} = \frac{\omega_N}{2H}, \tag{12}$$

where ζ denotes the damping ratio of the second-order response, while V_{cr} and V_{gr} represent the rated converter and PCC voltage, respectively. Note that in the implementation of the IEL, the magnitude of the reference voltage vector $\underline{v}_c^*$ output from the CC is used instead of its measured signal V_c. The inertial power P_H is then added onto the active power set-point of the converter, P_{set}, to form the reference power $P_g^\star$ for the APL, which can be effectively limited. The PI-based APL then tracks the power reference, $P_{lim}^\star$, and synchronizes the converter with the grid. Providing the inertia through the active-power reference allows a higher closed-loop bandwidth

[1]The VA corresponds to the inverse of the virtual impedance shown in Fig. 1.

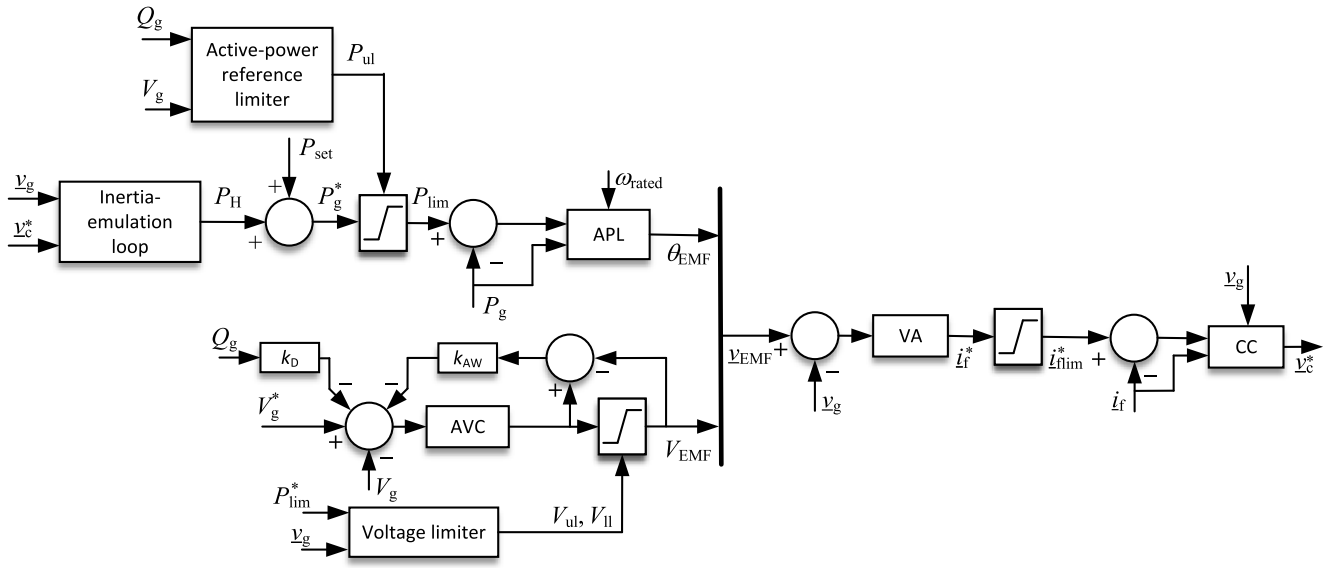

FIGURE 6. Block diagram of proposed control structure for GFM converters.

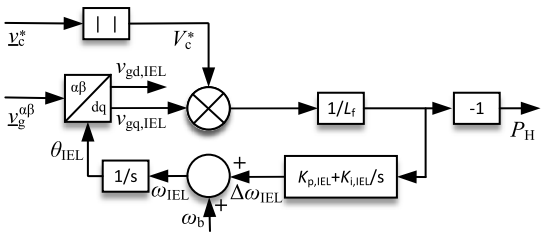

FIGURE 7. Block diagram of inertia emulation loop (IEL).

for the APL, thus making synchronization and reference tracking fast. Decoupling the synchronization task of the APL from the inertia provision gives the flexibility to limit and achieve a fast control over the active-power injection from the converter, and ultimately the resulting phase of the virtual back-EMF. The magnitude of the virtual back-EMF, V_{EMF}, can then be limited based on the available PCC voltage and estimated power flow as described in Section IV-C. In this way it is possible to limit the generated current reference vector without triggering the hard-current limiter.

B. CALCULATION OF ACTIVE-POWER LIMITS

As stated earlier, the phase of the virtual-back EMF is a resultant of the active-power flow from the converter. Therefore, setting the limits for the active-power reference would limit the resulting phase of the virtual-back EMF. During limitation, prioritizing active or reactive-power injection from the converter depends upon the grid-code requirements. Here, reactive-power injection is prioritized;[2] accordingly, the upper limit for the active-power reference, P_{ul}, is calculated as

$$P_{\text{ul}} = \sqrt{S_{\text{avail}}^2 - Q_{\text{g}}^2}, \tag{13}$$

where S_{avail} denotes the available apparent power of the converter, and Q_{g} is the reactive power injected from the converter (or, eventually, the reactive power demanded by the grid codes). At any time instant, depending upon the PCC-voltage magnitude, V_{g}, the available apparent power of the converter to keep the current within its rated value is calculated as $S_{\text{avail}} = \frac{S_{\text{N}} V_{\text{g}}}{V_{\text{N}}}$, where S_{N} and V_{N} denote the rated power and voltage of the converter, respectively. If $Q_{\text{g}} \geq S_{\text{avail}}$ (this condition prevails during a voltage dip for instance, when the converter current momentarily rises above its rated value), the upper limit for the active-power reference is set to zero.

C. CALCULATION OF VOLTAGE-MAGNITUDE LIMITS

The limits for the magnitude of virtual-back EMF can be calculated by using the estimated power flow. Considering the sign convention for the current in Fig. 1, a decrease in the PCC voltage will result in a positive reactive-power injection into the grid. Hence, the upper limit for the magnitude of the virtual-back EMF, V_{ul}, is calculated as

$$V_{\text{ul}} = \left| \underline{v}_{\text{g}} + \frac{P_{\text{lim}}^{\star} - jQ_{\text{avail}}}{\text{conj}(\underline{v}_{\text{g}})} (R_{\text{v}} + jX_{\text{v}}) \right|;$$
$$\text{with } Q_{\text{avail}} = \sqrt{S_{\text{avail}}^2 - P_{\text{lim}}^{\star 2}}. \tag{14}$$

Similarly, if a voltage swell at the PCC is to be considered, the lower limit for the virtual-back EMF, V_{ll}, can be calculated accordingly, i.e.,

$$V_{\text{ll}} = \left| \underline{v}_{\text{g}} + \frac{P_{\text{lim}}^{\star} + jQ_{\text{avail}}}{\text{conj}(\underline{v}_{\text{g}})} (R_{\text{v}} + jX_{\text{v}}) \right|. \tag{15}$$

[2]Prioritization of active and reactive power can be modified depending upon the system requirements.

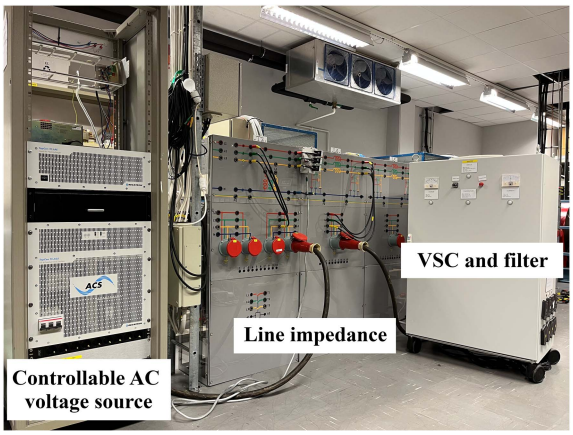

FIGURE 8. Photo of laboratory setup.

TABLE 1. System and Control Parameters

System parameters		Control parameters	
S_N	1 kVA	L_{v1}	0.35 pu
V_N	100 V	R_{v1}	0.235 pu
ω_N	314.16 rad/s	α_{PC}	2π 5 rad/s
L_f	0.15 pu	ζ	0.707
R_f	0.015 pu	α_{CC}	2π 500 rad/s
SCR	3	α_{VC}	2π 1 rad/s

It is worth mentioning here that during limitation, $P^{\star}_{\text{lim}}$ will be equal to P_{ul} as defined in (13). Thus, reactive-power injection is prioritized here. Furthermore, as $P_g = P^{\star}_{\text{lim}}$ during limitation, the angle of the voltage phasors $\underline{V}_{\text{ul}}$ and $\underline{V}_{\text{ll}}$ will be equal to zero in the controller's dq frame.

In order to prevent the accumulation of the voltage error during limitation, an anti-windup loop with the gain k_{AW} is implemented in the AVC as shown in Fig. 6.

V. EXPERIMENTAL VALIDATION OF PROPOSED CURRENT-LIMITATION STRATEGY

In order to validate the effectiveness of the proposed current-limitation strategy, experimental verification is made and discussed for various grid scenarios in this section. A photo of the laboratory setup is depicted in Fig. 8 and it resembles the system shown in Fig. 1. The grid is emulated using a REGATRON's four quadrant programmable AC power source. Furthermore, the GFM converter system used here comprises of a 2-level VSC supplied by an ideal DC voltage source. It is controlled using dSPACE dS1006, and is connected at the PCC through a phase reactor of resistance R_f and inductance L_f. Various system and control parameters used for the grid-interfaced converter system are shown in Table 1. The closed-loop bandwidths of the APL and AVC are chosen to comply with the recommendations for GFM control action defined in [47].

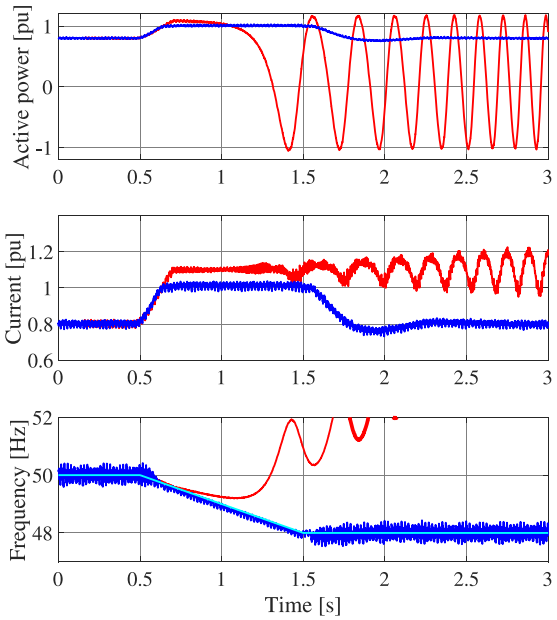

FIGURE 9. Dynamic response of GFM converter to a frequency disturbance with proposed control structure (blue curves), and Integrated GFM control (red curves). Top: measured active power; middle: measured converter-current magnitude; bottom: measured PCC frequency (light-blue curve depicts the frequency disturbance imposed by the controllable AC power source).

A. DYNAMIC PERFORMANCE IN CASE OF A ROCOF EVENT

In order to investigate the dynamic performance of the GFM converter system during a RoCoF event, the frequency, f_s, of the voltage source behind grid impedance is varied from 50.0 Hz to 48.0 Hz at a rate of −2.0 Hz/s between 0.5 s and 1.5 s. The active power set-point of the converter is selected as 0.8 pu in this case. The blue curves in Fig. 9 show the dynamic response of the converter system emulating an inertia of 5.0 s using the proposed control structure and current-limitation strategy. For comparison, the dynamic performance of a converter system emulating the same amount of inertia within the APL and deploying circular-current limitation (henceforth referred as *Integrated GFM control*[3]) is shown with red curves in Fig. 9, where the upper-limit for the hard-current limiter is set to 1.1 pu.

It can be seen from the figure that by using the proposed control structure and current-limitation strategy, it is possible to limit the converter current close to its rated value without triggering the hard-current limiter. Additionally, the internal frequency of the converter closely follows the declining grid frequency (light-blue curve), i.e., the converter keeps its synchronism with the grid. Furthermore, the active-power flow from the converter is limited close to 1.0 pu which otherwise would have reached 1.2 pu without limitation (corresponding to set-point power of 0.8 pu and inertial power of 0.4 pu). On

[3]The integrated GFM control used here for comparison corresponds to the structure displayed in Fig. 4, but provides inertia through the APL by proper selection of a lower APL bandwidth resulting in the desired inertia.

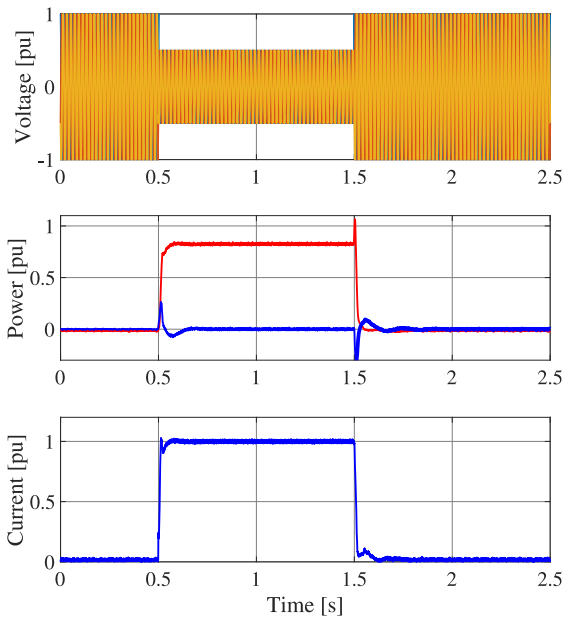

FIGURE 10. Dynamic response of GFM converter to a balanced three-phase voltage dip. Top: three-phase source voltage; middle: measured active (blue curve) and reactive power (red curve); bottom: measured converter-current magnitude.

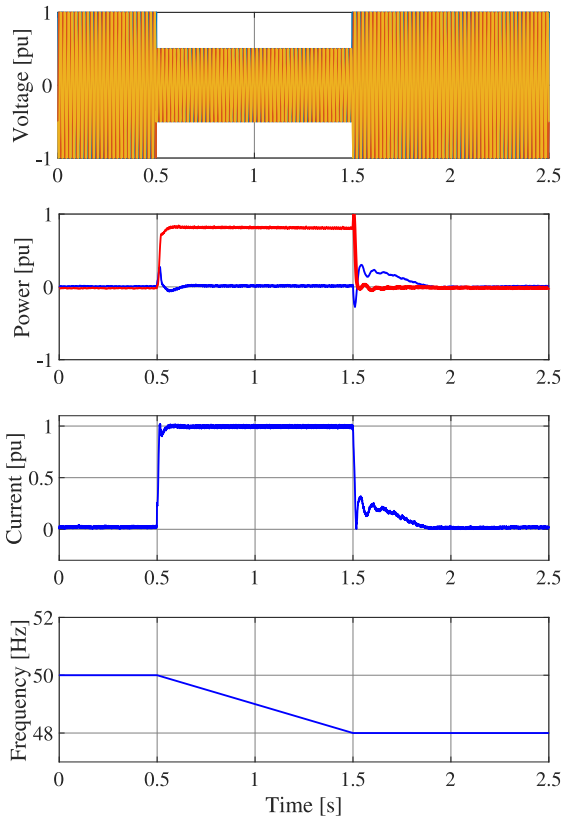

FIGURE 11. Dynamic response of GFM converter to a balanced three-phase voltage dip accompanied by a frequency disturbance. Top: three-phase source voltage; top-middle: measured active (blue curve) and reactive power (red curve); bottom-middle: measured converter-current magnitude; bottom: frequency disturbance imposed by the controllable AC power source.

the other hand, due to the presence of inertia within the APL in the second case, the converter loses it synchronism when the maximum-current limit of the converter is reached.

B. DYNAMIC PERFORMANCE IN CASE OF A BALANCED THREE-PHASE VOLTAGE DIP

In order to investigate the dynamic performance of the converter system during a balanced three-phase voltage dip, starting at 0.5 s, the magnitude of the source voltage, V_s, is reduced by 50% for a duration of 1.0 s. The set point for the active power is zero and inertia provision from the converter is minimized by deactivating the IEL for this case. Fig. 10 shows the dynamic response of the GFM converter system against a balanced three-phase voltage dip.

It can be seen from the figure that following the voltage dip, the converter current is immediately limited close to its rated value without triggering the hard-current limiter, thus, without changing the converter's dynamics. Additionally, maximum reactive power (red curve) is injected from the converter instantaneously to support the system. It can also be observed that after the fault clearance, the active and reactive powers as well as the converter current immediately return to their initial operating points.

C. DYNAMIC PERFORMANCE IN CASE OF A BALANCED THREE-PHASE VOLTAGE DIP ACCOMPANIED BY A ROCOF EVENT

In order to investigate the dynamic performance of the converter during a balanced three-phase voltage dip accompanied by a RoCoF event, V_s is reduced as in the previous case. At the same time, f_s is varied from 50.0 Hz to 48.0 Hz at a rate of -2.0 Hz/s. Such a severe event, comprising of a combination of large voltage and frequency disturbance, might happen in extreme system conditions like the system event reported in [48] or during the 2021 European system split between France and Spain [49], and is here used to test the capabilities and robustness of the suggested converter control. Fig. 11 shows the dynamic response of the GFM converter system emulating an inertia of 5.0 s for this case.

It can be observed from the figure that following the specified event, the converter current is immediately limited close to its rated value without triggering the hard-current limiter. Additionally, the converter injects maximum reactive power (red curve) instantaneously to support the system. Since the converter current reaches its rated value, there is no room for the active-power injection, and hence the active-power flow from the converter stays at zero. This results from the choice of prioritizing reactive power injection over active power made in (13). Since it's a matter of choice only, it is possible to reduce the reactive power injection if an inertial support is desired from the converter during limitation. It can also be observed that after the fault is cleared, the reactive power

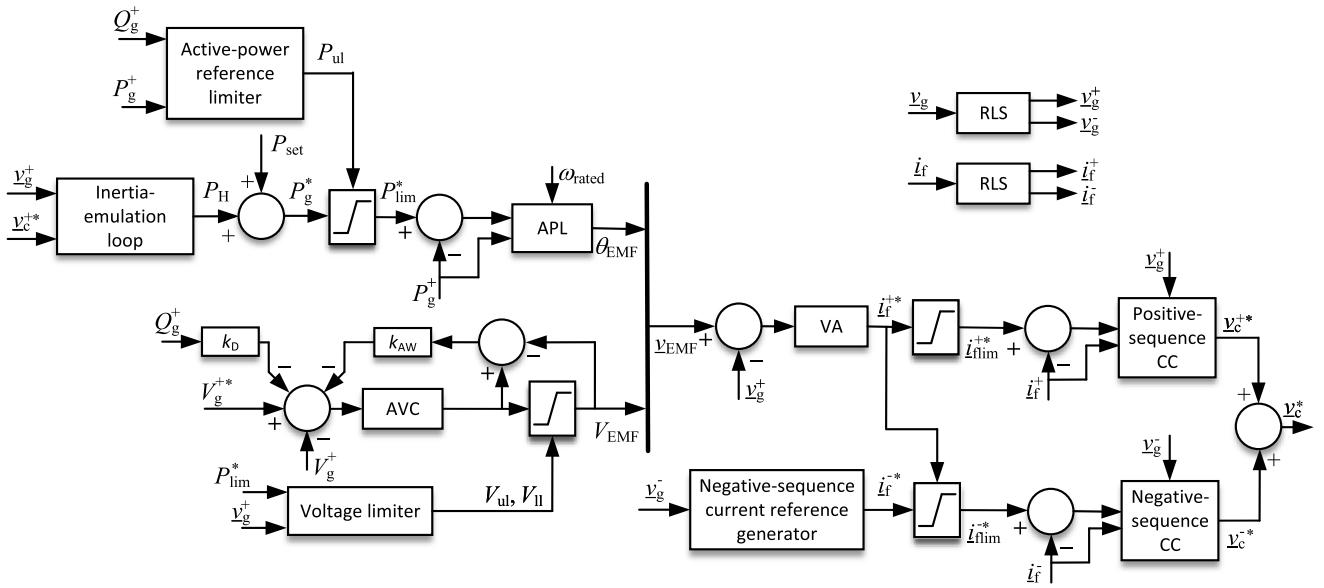

FIGURE 12. Block diagram of proposed control structure for GFM converters with adaptations for unbalanced grid conditions.

immediately returns to its initial operating point. Furthermore, the inertial response of the converter becomes evident from a decrease in the inertial power of the converter from the moment the frequency transient ends.

VI. CONTROLLER MODIFICATIONS FOR UNBALANCED GRID CONDITIONS

According to the latest reports from the European Network of Transmission System Operators for Electricity (ENTSO-e), the GFM converters should act as a sink for unbalances in the grid voltage [2]. This means that in case of unbalanced grid conditions (for example, during unbalanced faults), the converter must offer an inductive behavior towards the grid. As an example, the recent VDE-AR-N 4120 Technical Connection Rules establishes requirements for the negative-sequence current injection from the grid-connected converter systems [50]. In particular, for an unbalanced voltage dip the converter should absorb a negative-sequence current proportional to the negative-sequence grid voltage, following the relation

$$I_{\mathrm{f}}^{-} = k_{\mathrm{n}} V_{\mathrm{g}}^{-},\ 2 \le k_{\mathrm{n}} \le 6 \tag{16}$$

where the gain k_{n} specifies the relation between the magnitude of the negative-sequence component in the grid voltage, V_{g}^{-}, and the corresponding negative-sequence converter current I_{f}^{-}. During current limitation, prioritizing positive- or negative-sequence current depends upon the system requirements. This implies that we should be able to effectively control and limit both the positive- and negative-sequence currents individually. Fig. 12 shows the modifications made to the controller for this purpose, where a negative-sequence CC has been added to the original control structure. It generates a negative-sequence reference voltage for the converter, $\underline{v}_{\mathrm{c}}^{-\star}$, which is added to the positive-sequence reference voltage, $\underline{v}_{\mathrm{c}}^{+\star}$, generated by the original control structure.

During unbalanced grid conditions, the magnitude of the voltage and current vectors, as well as the instantaneous active and reactive powers will present oscillations at twice the fundamental frequency. This will lead to double-frequency oscillations in both the internal frequency of the converter and magnitude of the virtual-back EMF. To prevent this, positive-sequence components of the measured voltages and currents are used as inputs in the APL and AVC, while the negative-sequence components for the negative-sequence CC. In this article, Recursive Least Square (RLS) algorithm based method is used to separate the voltage and current vectors into their respective sequence components [51]. To adapt to the changes in the grid frequency, the internal frequency of the converter is used as an input to the RLS-based sequence separator.

In accordance with the relation between negative-sequence voltage and current provided in (16), the converter should exhibit negative-sequence reactance, $X_{\mathrm{n}} = k_{\mathrm{n}}^{-1}$. Therefore, the reference for the negative-sequence CC, $\underline{i}_{\mathrm{f}}^{-\star}$, is calculated as

$$\underline{i}_{\mathrm{f}}^{-\star} = \frac{\underline{v}_{\mathrm{g}}^{-}}{jX_{\mathrm{n}}}, \tag{17}$$

where $\underline{v}_{\mathrm{g}}^{-}$ represents the negative-sequence component of the PCC-voltage vector. The factor, k_{n}, is selected here equal to 2. Circular limitation is used here for the negative-sequence current in order to keep the total converter current within its rated value, I_{N}. Giving positive-sequence current priority for active and reactive-power support, the upper and lower limits for the magnitude of the negative-sequence current reference, denoted by $I_{\mathrm{f,ul}}^{-}$ and $I_{\mathrm{f,ll}}^{-}$, respectively, are calculated as

$$\begin{aligned} I_{\mathrm{f,ul}}^{-} &= I_{\mathrm{N}} - I_{\mathrm{f}}^{+\star}, \\ I_{\mathrm{f,ll}}^{-} &= -I_{\mathrm{f,ul}}^{-}. \end{aligned} \tag{18}$$

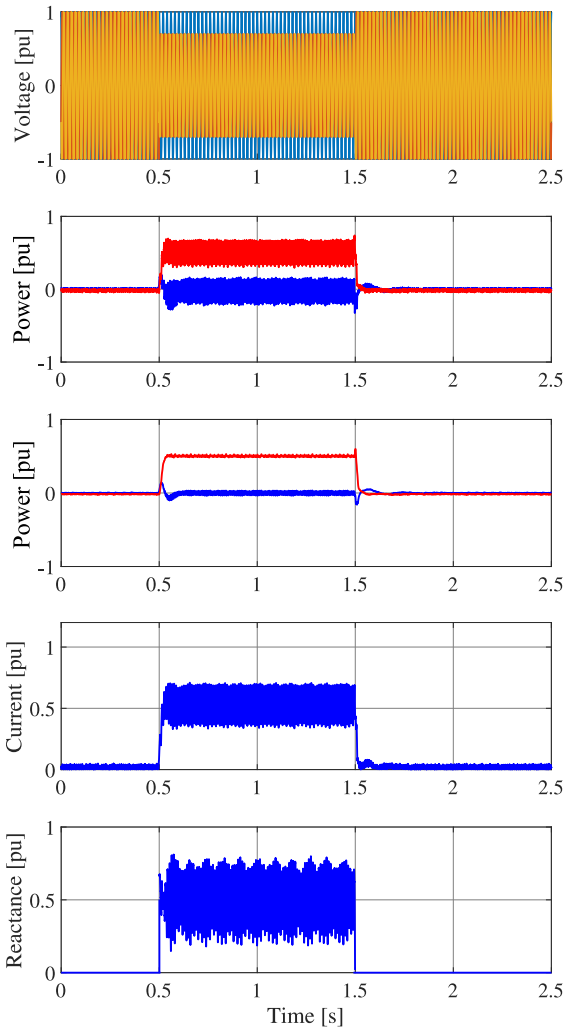

FIGURE 13. Dynamic response of GFM converter to a shallow unbalanced voltage dip. From top to bottom: three-phase source voltage, measured active (blue curve) and reactive power (red curve), measured positive-sequence active (blue curve) and reactive (red curve) power, measured converter-current magnitude, measured negative-sequence reactance of the converter.

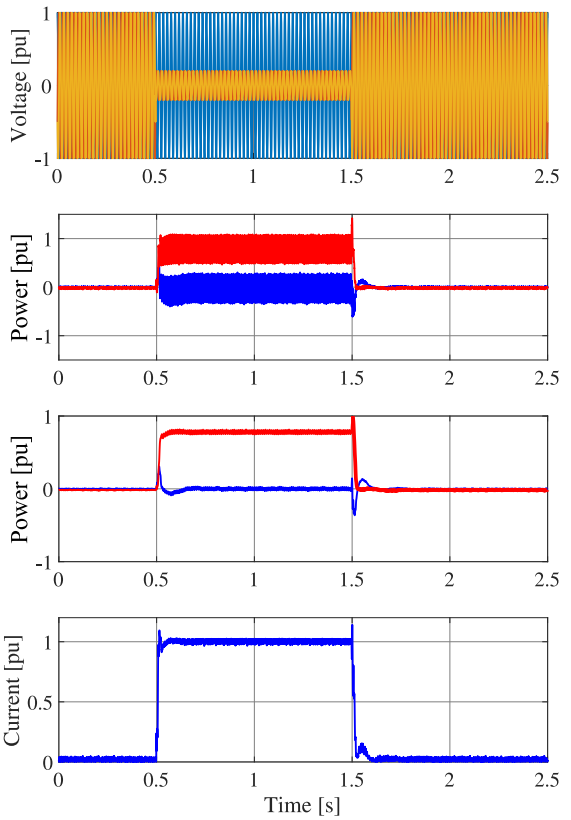

FIGURE 14. Dynamic response of GFM converter to a severe unbalanced voltage dip. From top to bottom: three-phase source voltage, measured active (blue curve) and reactive power (red curve), measured positive-sequence active (blue curve) and reactive (red curve) power, measured converter-current magnitude.

$I_{\mathrm{f}}^{+\star}$ denotes the magnitude of the positive-sequence current reference and is calculated as $I_{\mathrm{f}}^{+\star} = \sqrt{(i_{\mathrm{f,d}}^{+\star})^2 + (i_{\mathrm{f,q}}^{+\star})^2}$. During limitation, the magnitude of the negative-sequence current reference, $I_{\mathrm{f}}^{-\star}$, is saturated at its upper or lower limit according to (18). On the other hand, its phase angle, i.e., $\angle \underline{i}_{\mathrm{f}}^{-\star}$ is kept unchanged and is determined using (17).

A. EXPERIMENTAL VALIDATION UNDER UNBALANCED GRID CONDITIONS

The following test cases validate the effectiveness of the proposed limitation strategy during unbalanced grid conditions. The set point for the active-power flow from the converter is zero for the case studies presented here.

1) DYNAMIC PERFORMANCE IN CASE OF A SMALL UNBALANCE

In order to investigate the dynamic performance of the converter during a small unbalance, the magnitude of the source voltage in phase B and C is reduced by 30% for a duration of 1.0 s. Fig. 13 shows the dynamic response of converter system for this case.

It can be observed from the figure that following the specified disturbance, the converter injects reactive power (red curve) to boost the positive-sequence voltage at the PCC. Since $k_{\mathrm{n}} = 2$, the converter exhibits a negative-sequence reactance of 0.5 pu (calculated by dividing the measured negative-sequence voltage with resulting negative-sequence current during unbalance), hence allowing the negative-sequence current to flow. Furthermore, the positive sign of negative-sequence reactance confirms the inductive behavior of the converter to counter unbalance in the PCC voltage.

2) DYNAMIC PERFORMANCE IN CASE OF A SEVERE UNBALANCE

In order to investigate the dynamic performance of the converter against a severe unbalance, the magnitude of the source

voltage in phase B and C is reduced by 80% for a duration of 1.0 s. Fig. 14 shows the dynamic response of converter system for this case. It can be observed from the figure that giving positive-sequence current priority over the negative sequence results in an injection of maximum reactive power (red curve) from the converter. Since the converter current reaches its rated value, there is no room left for the negative-sequence current to flow, i.e, $\underline{i}_{\mathrm{f}}^{-\star}$ is automatically set to zero from (18). Consequently, the measured converter current is composed of positive-sequence component only unlike the current in Fig. 13, where the 100.0 Hz oscillation due to negative-sequence component is evident.

VII. CONCLUSION

In this article, a novel current limitation strategy for grid-forming converters has been presented. The existing current limitation strategies for GFM converters have been discussed, together with causes for instability in case of large disturbances. In order to guarantee converter's stability and at the same time preserve its GFM behavior also during current limitation, a novel limitation strategy has been presented. In the proposed strategy, current limitation is achieved by dynamically limiting the virtual-back EMF vector. Experimental results show the ability to effectively limit the current output of the converter to the desired value for several system events, without the need to activate the reference-current limiter at the input of the CC. Furthermore, modifications to cope with unbalanced grid conditions and fulfill the related grid codes have been presented.

REFERENCES

[1] United Nations Framework Convention on Climate Change, "Adoption of the Paris Agreement - 21st conference of the parties," Paris, 2015. [Online]. Available: https://unfccc.int/sites/default/files/english_paris_agreement.pdf

[2] ENTSO-E, "High penetration of power electronic interfaced power sources and the potential contribution of grid forming converters," 2020. [Online]. Available: https://eepublicdownloads.entsoe.eu/clean-documents/Publications/SOC/High_Penetration_of_Power_Electronic_Interfaced_Power_Sources_and_the_Potential_Contribution_of_Grid_Forming_Converters.pdf

[3] J. Matevosyan et al., "Grid-forming inverters: Are they the key for high renewable penetration?," *IEEE Power Energy Mag.*, vol. 17, no. 6, pp. 89–98, Nov./Dec. 2019.

[4] J. Rocabert, A. Luna, F. Blaabjerg, and P. Rodríguez, "Control of power converters in AC microgrids," *IEEE Trans. Power Electron.*, vol. 27, no. 11, pp. 4734–4749, Nov. 2012.

[5] S. D'Arco and J. A. Suul, "Virtual synchronous machines – classification of implementations and analysis of equivalence to droop controllers for microgrids," in *Proc. IEEE Grenoble Conf.*, 2013, pp. 1–7.

[6] H.-P. Beck and R. Hesse, "Virtual synchronous machine," in *Proc. 9th Int. Conf. Elect. Power Qual. Utilisation*, 2007, pp. 1–6. [Online]. Available: https://ieeexplore.ieee.org/document/4424220/

[7] Q. Zhong and G. Weiss, "Synchronverters: Inverters that mimic synchronous generators," *IEEE Trans. Ind. Electron.*, vol. 58, no. 4, pp. 1259–1267, Apr. 2011.

[8] A. Tayyebi, F. Dörfler, F. Kupzog, Z. Miletic, and W. Hribernik, "Grid-forming converters–inevitability, control strategies and challenges in future grids application," in *Proc. CIRED Workshop*, 2018, Paper no. 0236.

[9] R. Rosso, X. Wang, M. Liserre, X. Lu, and S. Engelken, "Grid-forming converters: Control approaches, grid-synchronization, and future trends – A review," *IEEE Open J. Ind. Appl.*, vol. 2, pp. 93–109, 2021. [Online]. Available: https://ieeexplore.ieee.org/document/9408354/

[10] B. Fan and X. Wang, "Current-limiting control of grid-forming inverters: State-of-the-art and open issues," [Online]. Available: https://www.techrxiv.org/articles/preprint/Current-Limiting_Control_of_Grid-Forming_Inverters_State-of-the-Art_and_Open_Issues/20430816/1

[11] B. Fan, T. Liu, F. Zhao, H. Wu, and X. Wang, "A review of current-limiting control of grid-forming inverters under symmetrical disturbances," *IEEE Open J. Power Electron.*, vol. 3, pp. 955–969, 2022.

[12] Enstore, "Enstore updated guide for GB Grid Forming Converters–V-005," 2021, [Online]. Available: https://www.nationalgrideso.com/industry-information/codes/grid-code-old/modifications/gc0137-minimum-specification-required

[13] NERC, "Grid forming technology - bulk power system reliability consideration," 2021. [Online]. Available: https://www.nerc.com/comm/RSTC_Reliability_Guidelines/White_Paper_Grid_Forming_Technology.pdf

[14] S. D'Arco, J. A. Suul, and O. B. Fosso, "Control system tuning and stability analysis of Virtual Synchronous Machines," in *Proc. IEEE Energy Convers. Congr. Expo.*, 2013, pp. 2664–2671.

[15] T. Qoria, F. Gruson, F. Colas, X. Guillaud, M.-S. Debry, and T. Prevost, "Tuning of cascaded controllers for robust grid-forming voltage source converter," in *Proc. Power Syst. Comput. Conf.*, 2018, pp. 1–7. [Online]. Available: https://ieeexplore.ieee.org/document/8443018/

[16] H. Deng, Y. Qi, J. Fang, Y. Tang, and V. Debusschere, "A robust low-voltage-ride-through strategy for grid-forming converters based on reactive power synchronization," *IEEE Trans. Power Electron.*, vol. 38, no. 1, pp. 346–357, Jan. 2023.

[17] P. Rodriguez, I. Candela, C. Citro, J. Rocabert, and A. Luna, "Control of grid-connected power converters based on a virtual admittance control loop," in *Proc. 15th Eur. Conf. Power Electron. Appl.*, 2013, pp. 1–10.

[18] M. G. Taul, X. Wang, P. Davari, and F. Blaabjerg, "Current limiting control with enhanced dynamics of grid-forming converters during fault conditions," *IEEE Trans. Emerg. Sel. Topics Power Electron.*, vol. 8, no. 2, pp. 1062–1073, Jun. 2020. [Online]. Available: https://ieeexplore.ieee.org/document/8779657/

[19] A. Narula, M. Bongiorno, M. Beza, and P. Chen, "Tuning and evaluation of grid-forming converters for grid-support," in *Proc. 23rd Eur. Conf. Power Electron. Appl.*, 2021, pp. P.1–P.10.

[20] K. G. Saffar, S. Driss, and F. B. Ajaei, "Impacts of current limiting on the transient stability of the virtual synchronous generator," *IEEE Trans. Power Electron.*, vol. 38, no. 2, pp. 1509–1521, Feb. 2023, [Online]. Available: https://ieeexplore.ieee.org/document/9899737/

[21] L. Zhang, L. Harnefors, and H. Nee, "Power-synchronization control of grid-connected voltage-source converters," *IEEE Trans. Power Syst.*, vol. 25, no. 2, pp. 809–820, May 2010.

[22] L. Harnefors, M. Hinkkanen, U. Riaz, F. M. M. Rahman, and L. Zhang, "Robust analytic design of power-synchronization control," *IEEE Trans. Ind. Electron.*, vol. 66, no. 8, pp. 5810–5819, Aug. 2019.

[23] F. Salha, F. Colas, and X. Guillaud, "Virtual resistance principle for the overcurrent protection of PWM voltage source inverter," in *Proc. IEEE PES Innov. Smart Grid Technol. Conf. Eur.*, 2010, pp. 1–6.

[24] J. He and Y. W. Li, "Analysis, design, and implementation of virtual impedance for power electronics interfaced distributed generation," *IEEE Trans. Ind. Appl.*, vol. 47, no. 6, pp. 2525–2538, Nov./Dec. 2011, [Online]. Available: https://ieeexplore.ieee.org/document/6022775/

[25] A. D. Paquette and D. M. Divan, "Virtual impedance current limiting for inverters in microgrids with synchronous generators," *IEEE Trans. Ind. Appl.*, vol. 51, no. 2, pp. 1630–1638, Mar./Apr. 2015.

[26] B. Wang, R. Burgos, and B. Wen, "Grid-forming inverter control strategy with improved fault ride through capability," in *Proc. IEEE Energy Convers. Congr. Expo.*, 2022, pp. 1–8.

[27] Z. Jin and X. Wang, "A DQ-Frame asymmetrical virtual impedance control for enhancing transient stability of grid-forming inverters," *IEEE Trans. Power Electron.*, vol. 37, no. 4, pp. 4535–4544, Apr. 2022.

[28] J. M. Bloemink and M. R. Iravani, "Control of a multiple source microgrid with built-in islanding detection and current limiting," *IEEE Trans. Power Del.*, vol. 27, no. 4, pp. 2122–2132, Oct. 2012.

[29] K. Shi, H. Ye, P. Xu, D. Zhao, and L. Jiao, "Low-voltage ride through control strategy of virtual synchronous generator based on the analysis of excitation state," *IET Gener., Transmiss. Distrib.*, vol. 12, no. 9, pp. 2165–2172, 2018. [Online]. Available: https://onlinelibrary.wiley.com/doi/abs/10.1049/iet-gtd.2017.1988

[30] J. Chen, F. Prystupczuk, and T. O'Donnell, "Use of voltage limits for current limitations in grid-forming converters," *CSEE J. Power Energy Syst.*, vol. 6, no. 2, pp. 259–269, 2020.
[31] E. Afshari et al., "Control strategy for three-phase grid-connected PV inverters enabling current limitation under unbalanced faults," *IEEE Trans. Ind. Electron.*, vol. 64, no. 11, pp. 8908–8918, Nov. 2017.
[32] P. Piya, M. Ebrahimi, M. Karimi-Ghartemani, and S. A. Khajehoddin, "Fault ride-through capability of voltage-controlled inverters," *IEEE Trans. Ind. Electron.*, vol. 65, no. 10, pp. 7933–7943, Oct. 2018.
[33] L. Huang, L. Zhang, H. Xin, Z. Wang, and D. Gan, "Current limiting leads to virtual power angle synchronous instability of droop-controlled converters," in *Proc. IEEE Power Energy Soc. Gen. Meeting*, 2016, pp. 1–5.
[34] H. Xin, L. Huang, L. Zhang, Z. Wang, and J. Hu, "Synchronous instability mechanism of P-F droop-controlled voltage source converter caused by current saturation," *IEEE Trans. Power Syst.*, vol. 31, no. 6, pp. 5206–5207, Nov. 2016.
[35] H. Lin, C. Jia, J. M. Guerrero, and J. C. Vasquez, "Angle stability analysis for voltage-controlled converters," *IEEE Trans. Ind. Electron.*, vol. 64, no. 8, pp. 6265–6275, Aug. 2017.
[36] T. Qoria, F. Gruson, F. Colas, G. Denis, T. Prevost, and X. Guillaud, "Critical clearing time determination and enhancement of grid-forming converters embedding virtual impedance as current limitation algorithm," *IEEE Trans. Emerg. Sel. Topics Power Electron.*, vol. 8, no. 2, pp. 1050–1061, Jun. 2020. [Online]. Available: https://ieeexplore.ieee.org/document/8931732/
[37] T. Qoria, F. Gruson, F. Colas, X. Kestelyn, and X. Guillaud, "Current limiting algorithms and transient stability analysis of grid-forming VSCs," *Electric Power Syst. Res.*, vol. 189, 2020, Art. no. 106726. [Online]. Available: https://www.sciencedirect.com/science/article/pii/S0378779620305290
[38] X. Wang, M. G. Taul, H. Wu, Y. Liao, F. Blaabjerg, and L. Harnefors, "Grid-synchronization stability of converter-based resources–An overview," *IEEE Open J. Ind. Appl.*, vol. 1, pp. 115–134, 2020.
[39] D. Pan, X. Wang, F. Liu, and R. Shi, "Transient stability of voltage-source converters with grid-forming control: A design-oriented study," *IEEE Trans. Emerg. Sel. Topics Power Electron.*, vol. 8, no. 2, pp. 1019–1033, Jun. 2020.
[40] E. Rokrok, T. Qoria, A. Bruyere, B. Francois, and X. Guillaud, "Transient stability assessment and enhancement of grid-forming converters embedding current reference saturation as current limiting strategy," *IEEE Trans. Power Syst.*, vol. 37, no. 2, pp. 1519–1531, Mar. 2022.
[41] P. Imgart, A. Narula, M. Bongiorno, M. Beza, and J. R. Svensson, "A cascaded power controller for robust frequency ride-through of grid-forming converters," in *Proc. IEEE Energy Convers. Congr. Expo.*, 2022, pp. 1–8.
[42] J. Alipoor, Y. Miura, and T. Ise, "Power system stabilization using virtual synchronous generator with alternating moment of inertia," *IEEE Trans. Emerg. Sel. Topics Power Electron.*, vol. 3, no. 2, pp. 451–458, Jun. 2015.
[43] H. Wu and X. Wang, "A mode-adaptive power-angle control method for transient stability enhancement of virtual synchronous generators," *IEEE Trans. Emerg. Sel. Topics Power Electron.*, vol. 8, no. 2, pp. 1034–1049, Jun. 2020.
[44] A. Narula, M. Bongiorno, and M. Beza, "Comparison of grid-forming converter control strategies," in *Proc. IEEE Energy Convers. Congr. Expo.*, 2021, pp. 361–368.
[45] "Västerås: Applied Signal Processing and Control," Dept. Electron., Mälardalen Univ., 2002. [Online]. Available: http://libris.kb.se/bib/10894706
[46] R. Rosso, M. Andresen, S. Engelken, and M. Liserre, "Analysis of the interaction among power converters through their synchronization mechanism," *IEEE Trans. Power Electron.*, vol. 34, no. 12, pp. 12321–12332, Dec. 2019.
[47] National Grid ESO, "Minimum specification required for provision of GB grid forming (GBGF) capability," Tech. Rep. GC0137, 2021. [Online]. Available: https://www.nationalgrideso.com/document/220511/download
[48] Australian Energy Market Operator, "Trip of multiple generators and lines in Central Queensland and associated under-frequency load shedding on 25 May 2021," 2021. [Online]. Available: https://aemo.com.au/-/media/files/electricity/nem/market_notices_and_events/power_system_incident_reports/2021/final-report-trip-of-multiple-generators-and-lines-in-qld-and-under-frequency-load-shedding.pdf?la=en
[49] ENTSO-E, "Continental europe synchronous area separation on 24 July 2021 - technical report," 2021. [Online]. Available: https://eepublicdownloads.entsoe.eu/clean-documents/SOC%20documents/SOC%20Reports/entso-e_CESysSep_210724_211112.pdf
[50] Verband der Elektrotechnik Elektronik Informationstechnik e. V., *Tech. Connection Rules for High-Voltage (VDE-AR-N 4120)*, 2018. [Online]. Available: https://www.vde.com/en/fnn/topics/technical-connection-rules/tar-for-high-voltage
[51] M. Beza and M. Bongiorno, "Application of recursive least squares algorithm with variable forgetting factor for frequency component estimation in a generic input signal," *IEEE Trans. Ind. Appl.*, vol. 50, no. 2, pp. 1168–1176, Mar./Apr. 2014.

ANANT NARULA (Student Member, IEEE) received the M.Sc. degree in smart electrical networks and systems (EIT InnoEnergy) from the KTH Royal Institute of Technology, Stockholm, Sweden, and Universitat Politècnica de Catalunya, Barcelona, Spain, in 2018. He is currently working toward the Ph.D. degree with the Chalmers University of Technology, Göteborg, Sweden. His research interest includes application of power electronics in power systems and stability studies of power system.

PAUL IMGART (Student Member, IEEE) received the B.Sc. and M.Sc. degrees in power engineering from Leibniz University Hannover, Hannover, Germany. He is currently working toward the Ph.D. degree with the Chalmers University of Technology, Göteborg, Sweden. His research interests include stability and robustness of sustainable power grids, with particular focus on innovative converter control strategies for converter-dominated systems.

MASSIMO BONGIORNO (Senior Member, IEEE) received the M.Sc. degree in electrical engineering from the University of Palermo, Palermo, Italy, in April 2002, and the Lic. Eng. and Ph.D. degrees in electric power engineering from the Chalmers University of Technology, Gothenburg, Sweden, in December 2004 and September 2007, respectively. From 2007 to 2010, he was an Assistant Professor with the Department of Electric Power Engineering, Chalmers University of Technology, where he became an Associate Professor in 2010. Since 2015, he has been holding the position of a Professor in power electronic applications for power systems and he has been the Head of the Division of electric power engineering with the Chalmers University of Technology since 2020. His research interests include the application of power electronics in power systems, converter control, power system dynamics, and power quality.

MEBTU BEZA (Member, IEEE) received the B.Sc. degree in electrical engineering with Bahir Dar University, Bahir Dar, Ethiopia, in July 2005, and the M.Sc., Lic. Eng., and Ph.D. degrees in electric power engineering and the D.Sc. degree (Docent) in control and modeling of power electronic converters in power systems from the Chalmers University of Technology, Gothenburg, Sweden, in June 2009, June 2012, February 2015, and October 2020, respectively. He is currently a Specialist Researcher with the Chalmers University of Technology. His research interests include signal processing in power systems, control theory, stability studies in converter-dominated systems, and application of power electronics in power systems.

JAN R. SVENSSON (Senior Member, IEEE) received the Ph.D. and D.Sc. degrees (Docent) in electric power engineering from Chalmers University of Technology, Göteborg, Sweden, in 1988 and 2002, respectively. From 1999 to 2009, he was with ABB in R&D of HVDC transmission, STATCOMs, and energy storages, especially design and control of light-concept devices (HVDC and FACTS). Between 2009 and 2014, he was the Program Manager for the global R&D Program Active Grid Infrastructure with ABB Corporate Research. From 2014 to 2020, he was a Senior Principal Scientist on power electronics systems with ABB Power Grids Research. He is also a Research Fellow with Hitachi Energy Research, Västerås, Sweden. Since 2018, he has been an Adjunct Professor with Chalmers University of Technology, Gothenburg, Sweden. His interests include design and control of power electronics in power systems, power quality, storage technologies, and renewable energy.

JEAN-PHILIPPE HASLER received the M.Sc. degree in electrical engineering from the Ecole Polytechnique Fédérale de Lausanne, Lausanne, Switzerland, in 1986. In 1986, he joined BBC, where he was developing control systems and protection algorithms for multi-terminal HVDC. Since 1993, he has been with ABB, conducting power system and control studies for different FACTS applications. Since 2014, he has been with ABB, where he is currently a Senior Principal Engineer with Hitachi Energy, Västerås, Sweden.